Molecular Biology of the Cell
Vol. 19, 2857–2869, July 2008

A Raft-derived, Pak1-regulated Entry Participates in α2β1 Integrin-dependent Sorting to Caveosomes

Mikko Karjalainen,*† Elina Kakkonen,*† Paula Upla,* Heli Paloranta,* Pasi Kankaanpää,‡ Prisca Liberali,§ G. Herma Renkema,‖ Timo Hyypiä,¶ Jyrki Heino,‡ and Varpu Marjomäki*

*Department of Biological and Environmental Science/Nanoscience Center, University of Jyväskylä, FI-40351 Jyväskylä, Finland; ‡Department of Biochemistry, University of Turku, FI-20014 Turku, Finland; §Department of Cell Biology and Oncology, Consorzio Mario Negri Sud, 66030 Santa Maria Imbaro (Chieti), Italy; ‖Institute of Medical Technology, University of Tampere and Tampere University Hospital, FI-22014 Tampere, Finland; and ¶Department of Virology, University of Turku, FI-20520 Turku, Finland

Submitted October 31, 2007; Revised April 15, 2008; Accepted April 22, 2008
Monitoring Editor: Jean Gruenberg

We have previously shown that a human picornavirus echovirus 1 (EV1) is transported to caveosomes during 2 h together with its receptor α2β1 integrin. Here, we show that the majority of early uptake does not occur through caveolae. α2β1 integrin, clustered by antibodies or by EV1 binding, is initially internalized from lipid rafts into tubulovesicular structures. These vesicles accumulate fluid-phase markers but do not initially colocalize with caveolin-1 or internalized simian virus 40 (SV40). Furthermore, the internalized endosomes do not contain glycosylphosphatidylinositol (GPI)-anchored proteins or flotillin 1, suggesting that clustered α2β1 integrin does not enter the GPI-anchored protein enriched endosomal compartment or flotillin pathways, respectively. Endosomes mature further into larger multivesicular bodies between 15 min to 2 h and concomitantly recruit caveolin-1 or SV40 inside. Cell entry is regulated by p21-activated kinase (Pak)1, Rac1, phosphatidylinositol 3-kinase, phospholipase C, and actin but not by dynamin 2 in SAOS-α2β1 cells. An amiloride analog, 5-(*N*-ethyl-*N*-isopropanyl) amiloride, blocks infection, causes integrin accumulation in early tubulovesicular structures, and prevents their structural maturation into multivesicular structures. Our results together suggest that α2β1 integrin clustering defines its own entry pathway that is Pak1 dependent but clathrin and caveolin independent and that is able to sort cargo to caveosomes.

INTRODUCTION

We have shown previously that echovirus 1 (EV1), a small nonenveloped RNA-containing picornavirus that binds specifically to α2β1 integrin on the plasma membrane, is internalized with this receptor into caveosomes (Marjomäki *et al*., 2002; Upla *et al*., 2004). EV1 binding to the α2β1 integrin induces protein kinase C (PKC)α activation, which is needed for the rapid delivery of EV1 and integrin to the caveosomes (Pelkmans *et al*., 2001; Pietiäinen *et al*., 2004; Upla *et al*., 2004). PKC activation and caveosomal targeting can be mimicked by clustering α2β1 integrin with a sequential treatment of specific primary and secondary antibodies (Upla *et al*., 2004). Caveosomes show complex morphology, high concentration of caveolin-1, and lack markers of the clathrin-dependent and secretory pathways (Pelkmans *et al*., 2001; Marjomäki *et al*., 2002; Pietiäinen *et al*., 2004). Our recent coinfection study with EV1 and simian virus 40 (SV40) indicated that both viruses can be found in the same caveosomal structures in CV-1 and SAOS-α2β1 cells but that their intracellular transport after this step differs remarkably: SV40 is routed to the endoplasmic reticulum, whereas EV1 has not been found to be transported to other cellular structures (Pietiäinen *et al*., 2004). Live cell imaging also suggested that the entry pathways of these two viruses into the caveosomes may be different because SV40 needed more time to reach the caveosomes, and, during the first few minutes of infection, EV1 was not efficiently recruited into the caveolae structures on the plasma membrane (Pietiäinen *et al*., 2004). These results led us to search for the early entry pathways that direct EV1 and α2β1 integrin to caveosomes.

Recent studies have suggested that, besides the clathrin- and caveolae-dependent routes, there exist several other internalization pathways that might differ only slightly from each other (Conner and Schmid, 2003; Kirkham and Parton, 2005; Marjomäki and Schaible, 2005; Marsh and Helenius, 2006; Mayor and Pagano, 2007). Efficient membrane and fluid uptake has been suggested to occur through these pathways. They include at least the dynamin-dependent pathway used by interleukin-2 receptor and dynamin-independent pathways, such as macropinocytosis and pathways used by glycosyl phosphatidylinositol-anchored proteins (GPI-APs), flotillins 1 and -2, and cholera toxin B (CTxB) subunit. Vesicles responsible for the traffic in these pathways have often been suggested to fuse with endosomes of the

This article was published online ahead of print in *MBC in Press* (http://www.molbiolcell.org/cgi/doi/10.1091/mbc.E07–10–1094) on April 30, 2008.

† These authors contributed equally to this work.

Address correspondence to: Varpu Marjomäki (vmarjoma@cc.jyu.fi).

Abbreviations used: CTxB, cholera toxin B; EV1, echovirus 1; GPI-AP, glycosyl phosphatidylinositol-anchored protein; SV40, simian virus 40; Pak, p21-activated kinase; HRP, horseradish peroxidase, PFA, paraformaldehyde.

clathrin route (Kirkham and Parton, 2005). In contrast, less is known about sorting into caveosomes by any other routes than along the caveolae pathway.

In this study, we have carefully followed the early steps of EV1 infection, including the uptake and subsequent delivery of the cargo into caveosomes. The transport of $\alpha2\beta1$ integrin and EV1 was examined in detail by electron and confocal microscopy and regulation of the initial entry pathway was analyzed.

MATERIALS AND METHODS

Cells, Viruses, Antibodies, and Reagents

Experiments were performed using a human osteosarcoma cell line, overexpressing the $\alpha2$ integrin subunit (SAOS-$\alpha2\beta1$ cells; Ivaska *et al*., 1999) and HeLa MZ cells (from Dr. Urs Greber, University of Zurich, Switzerland). EV1 (Farouk strain; American Type Culture Collection) was produced and purified as described previously (Marjomäki *et al*., 2002). SV40 was produced and purified as described previously (Pietiäinen *et al*., 2004). The conjugation of SV40 to Alexa 568 (Invitrogen, Carlsbad, CA) was performed as described previously (Pietiäinen *et al*., 2004). In parallel, SV40-Alexa Fluor conjugates from the laboratory of Prof. Ari Helenius (ETH Zürich, Switzerland) were used. In the conjugation, a low amount of succinimidyl ester dye was used that did not affect the SV40 infectivity. The following antibodies were used: rabbit antisera against purified EV1 (Marjomäki *et al*., 2002), caveolin-1 (N20 antibody; Santa Cruz Biotechnology, Santa Cruz, CA) and cation-independent mannose-6-phosphate receptor (CI-MPR) (Marjomäki *et al*., 1990), peptide antibodies against the conserved sequence of picornavirus 3D polymerase (Auvinen *et al*., 1993), p21-activated kinase (Pak)1 (Millipore Bioscience Research Reagents, Temecula, CA), phospho-Pak1 (Thr212; Genway, San Diego, CA), phospho-Pak1/2/3 (Ser141; BioSource International, Camarillo, CA), and monoclonal antibodies against $\alpha2$ integrin (MCA2025; Serotec, Oxford, United Kingdom; HAS6 from Fiona M. Watt, Cancer Research, London, United Kingdom; A211E10 from Dr. Fedor Berditchevski, Institute of Cancer studies, Birmingham, United Kingdom), Rac1 (Millipore, Billerica, MA), myc peptide (produced from 9E10 hybridoma cells; American Type Culture Collection), CD63 (Zymed Laboratories, South San Francisco, CA), early endosome antigen 1 (EEA1; BD Biosciences Transduction Laboratories, Lexington, KY), and FLAG peptide (Sigma-Aldrich, St. Louis, MO). Tetramethylrhodamine B isothiocyanate (TRITC)-labeled phalloidin was from Sigma-Aldrich, and 10-kDa fluorescent dextrans were from Invitrogen. Cholera toxin B subunit (1 μg/ml; Sigma-Aldrich) was bound on cells for 1 h on ice. Cells were pretreated with 100 μg/ml cycloheximide (Sigma-Aldrich) for 4 h before the experiment, and it was also present during the rest of the experiment. LysoTracker Red DND99 (100 nM; Invitrogen) was added to cells for 30 min at 37°C. Dynasore ($C_{18}H_{14}N_2O_4$; synthesized by Dr. Henry E. Pelish, provided by the Kirchhausen Lab, Immune Disease Institute, Boston, MA) was used at final concentration of 80 μM in serum-free DMEM with 30- and 60-min preincubation.

Transfections

Subconfluent SAOS-$\alpha2\beta1$ cells were transfected with an expression plasmid mixed with FuGENE 6 reagent (Roche Diagnostics, Indianapolis, IN). The cells were used for experiments after an expression time of 48 h. The following plasmids were used in the experiments: green fluorescent protein (GFP) construct of caveolin-1 (cav-GFP) and GPI-anchored GFP (GPI-GFP) were from Dr. Lucas Pelkmans (ETH Zürich, Switzerland), dynamin 2 constructs (wild-type [WT] and K44A mutant) and dynamin 2 polyclonal antibody were from Mark McNiven (Mayo Clinic College of Medicine, Rochester, MN). Pak1T423E myc construct was from Dr. Jonathan Chernoff (Fox Chase Cancer Center, Philadelphia, PA) and flag-tagged Pak1AID was from Dr. Ed Manser (GSK-IMCB Laboratory, Singapore). Cdc42 WT was from Dr. Lucas Pelkmans (ETH Zürich), Cdc42 and Rac1 mutants (17N) were from Dr. Johan Peränen, (University of Helsinki, Finland), and the myc-tagged Rac1 WT construct was from Dr. Herma Renkema (IMT, University of Tampere, Finland). Hemagglutinin-tagged constructs of WT-caveolin-3, caveolin-3-DGV, and caveolin-3-KSY were from Dr. Rob Parton (University of Queensland, Australia).

Small Interfering RNA (siRNA) Experiments

siRNAs against Rac1 (5′-CACCACUGUCCCAACACUCTT-3′), Cdc42 (5′-GAUAACUCACCACUGUCCATT-3′), RhoA (5′-GAAGUCAAGCAUUUCUGUCTT-3′), and dynamin 2 (SMARTpool) were from Dharmacon RNA Technologies (Lafayette, CO). Nonspecific siRNA (Dharmacon RNA Technologies) was used as a negative control, whereas siGLO (Dharmacon RNA Technologies) was used as a transfection marker. SAOS-$\alpha2\beta1$ cells were transfected using Oligofectamine (Invitrogen) according to the manufacturer's recommendations in the presence of siRNAs.

Viral Infection and Integrin Clustering Experiments

For EV1 infection, multiplicity of infection 100 was used in all experiments. EV1 was first bound to cells for 1 h on ice in DMEM (containing 1% serum), cells were washed extensively, and then they were put to 37°C to allow internalization. $\alpha2\beta1$ integrin clustering was done as described previously (Upla *et al*., 2004). Briefly, specific nonfunctional antibody (e.g., HAS6 or A211E10) against $\alpha2\beta1$ integrin was bound for 1 h on ice. Cells were washed extensively and incubated with a clustering secondary antibody (e.g., goat anti-mouse Alexa 488). After washing, the cells were incubated in DMEM (with 10% serum) at 37°C to allow internalization.

Transferrin and Dextran Uptake Assays

Transferrin, conjugated to Alexa 488 or Alexa 633 (Invitrogen) were internalized at 0.25 mg/ml concentration (in 1% DMEM) in cells for 1 h. Cells were washed extensively on ice with phosphate-buffered saline (PBS) containing 0.2% bovine serum albumin before fixation in 4% paraformaldehyde (PFA) for 30 min.

Dextran (10 kDa) conjugated to rhodamine, rhodamine green (lysine fixable), or fluorescein isothiocyanate (FITC) (lysine fixable; Invitrogen) were used at 0.25 or 1 mg/ml concentration. Internalization was performed continuously for 1–2 h or using 1-h pulse followed by 1-h chase (without the dextran), washed extensively as described above, and fixed with 4% PFA.

Drug Treatments

The following drugs were used: 100 μM 5-(*N*-ethyl-*N*-isopropanyl) amiloride (EIPA; Sigma-Aldrich), 50 μM LY294002 (Calbiochem, San Diego, CA), and 10 μM U73122 (Calbiochem). Cytotoxicity against these drugs was tested by the CellTiter 96AQueousOneSolutionAssay according to manufacturer's protocol (Promega. Madison, WI).

Immunofluorescence and Confocal Microscopy

Cells were fixed with 4% PFA, permeabilized with 0.1–0.2% Triton X-100 in PBS for 5 min, and treated with antibodies diluted in PBS containing 3% bovine serum albumin. Highly precross-absorbed goat secondary antibodies (conjugated to Alexa dyes 488, 555, and 633) against rabbit and mouse antibodies (Invitrogen) were used. The cells were mounted in Mowiol and examined with an Axiovert 100 M SP epifluorescence microscope (Carl Zeiss, Jena, Germany) equipped with a confocal setup (LSM510; Carl Zeiss) or with an Olympus microscope IX81 with a Fluoview-1000 confocal setup.

Differential labeling of the surface and intracellular ligands were done as described previously (Upla *et al*., 2004). Briefly, cells were incubated with EV1 for 2 h and fixed with 3% paraformaldehyde for 20 min. After fixation, EV1 was labeled without permeabilization by using a primary antibody and then the anti-rabbit Alexa 555 conjugate. After a 5-min permeabilization with 0.2% Triton X-100, again EV1 was labeled but now using anti-rabbit Alexa 488 conjugate. Thus, plasma membrane-associated EV1 was stained with both Alexa 555 and 488 conjugates, and it was seen as yellow when the red and green channels were merged. Green signal alone representing internalized EV1 was measured. The double-labeled cells were imaged as z-stack with the confocal microscope. In parallel experiments, the clusters of $\alpha2\beta1$ integrins were allowed to form in the presence of Alexa-conjugated secondary antibody and to be internalized. Samples were fixed as described above. The internalized integrins had green color, and the plasma membrane-associated integrins were labeled with Alexa 555 conjugate. Again yellow color in merge images represented integrin clusters on the plasma membrane and green signal alone represented internalized clusters.

Data Analysis of the Microscopic Data

Quantification of internalization and colocalization was determined with a free, open source software package, BioImageXD (Kankaanpää *et al*., 2006). To quantify the level of colocalization, 30 cells from three independent experiments, 10 cells from each experiment, were randomly selected and optically sectioned using confocal microscope. Levels for the laser power, detector amplification, and optical sections were optimized for each channel before starting the quantification. Colocalization was evaluated from the center slice of the cell by examination of the merged images and analysis was performed with BioImageXD. The colocalization thresholds were set manually so that background fluorescence and fluorescence from diffuse stain were eliminated. Overlap between channels was expressed as percentage Ch2 voxels colocalizing with Ch1 voxels. Statistical significance of observed colocalization was calculated by Costes algorithm (Costes *et al*., 2004), embedded in software, and only colocalization with zero coincidence probability were taken into account (i.e., $p = 1.000$).

BioImageXD contains a simple algorithm for calculating the ratio of surface/internalized virus. The formula is $Ch1/(Ch2 - Coloc)$, where Ch1 is number of voxels stained before permeabilization, Ch2 is number of voxels stained after permeabilization, and Coloc is number of colocalized voxels. Only voxels with intensity values above thresholds were considered for each of the three values. The thresholds were determined as described above.

The amount of dextran and transferrin in cells was determined by intensity threshold segmentation. The threshold was selected so that only clear intra-

cellular structures were visible. Connected component labeling algorithm was used to eliminate structures less than 3 voxels.

SDS-Polyacrylamide Gel Electrophoresis (PAGE) and Immunoblotting

Samples were separated in 12% SDS-polyacrylamide gel and electroblotted onto polyvinylidene difluoride membrane (Millipore). Primary antibodies and horseradish peroxidase conjugated secondary antibodies (Bio-Rad, Hercules, CA) were used. Bands were detected by chemiluminescence (Pierce Chemical, Rockford, IL).

Electron Microscopy

For visualizing the internalized $\alpha2\beta1$ integrin, cells were incubated with anti $\alpha2$ antibody (HAS6) and subsequently with rabbit anti-mouse IgG and protein A gold, and processed for electron microscopy (EM) as described previously (Upla *et al.*, 2004). In horseradish peroxidase (HRP) labeling experiments, the cells were incubated for 5–15 min at 37°C in complete culture medium containing 10 mg/ml HRP (HRP, type II; Sigma-Aldrich). After the experiments, the cells were fixed in 4% PFA containing 0.1% glutaraldehyde in 50 mM Tris buffer, pH 7.6, at room temperature for 1 h or at 4°C overnight. HRP was detected by incubating the cells first for 30 min with 0.1% diaminobenzidine (Sigma-Aldrich), and then again with the same mixture supplemented with 0.1% hydrogen peroxide for further 30 min. For immuno-EM cells were briefly fixed by 4% PFA, shortly treated by 0.1% Triton X-100 in PBS, and then incubated with rabbit antibodies against caveolin-1 (N20) for 1 h. Cells were then washed, treated with protein A gold for 2 h, washed, postfixed, and processed for EM (Upla *et al.*, 2004).

Ruthenium red staining was done as described previously (Liberali *et al.*, 2008). Briefly, after the internalization with integrin, cells were washed in cacodylate buffer, pH 7.3, fixed, and stained with 1.3% glutaraldehyde containing 0.07 mg/ml ruthenium red in cacodylate buffer for 1 h at room temperature. The cells were postfixed with 1.7% osmium tetroxide containing 0.07 mg/ml ruthenium red in cacodylate buffer for 3 h at room temperature. Cells were then dehydrated, stained with 2% uranyl acetate, and embedded in LX-112 Epon.

Statistical Testing

A t-test was used for pairwise statistical comparison between samples. For percentages or ratio figures, a *t* test was applied after arcsine $\sqrt{}$ transformation of the original variable to convert the binomial distribution of the data to follow normal distribution. Testing the means between samples in EM, binomial *t* test was applied.

RESULTS

$\alpha2\beta1$ Integrin Clustering Sorts EV1 and Fluid-Phase Markers from the Cell Surface to Caveosomes

We have previously shown that during EV1 infection, the virus particles and their receptor $\alpha2\beta1$ integrin accumulate in caveosomes during the first 2 h of infection (Marjomäki *et al.*, 2002; Upla *et al.*, 2004). However, our previous imaging of live cells expressing caveolin-GFP suggested that EV1 does not colocalize with caveolin-1 on the plasma membrane during the first minutes of receptor interaction, suggesting that EV1 is not mainly internalized via caveolae (Pietiäinen *et al.*, 2004). In this study, we wanted to characterize the earliest steps of the entry pathway that lead to the caveosomes; therefore, we followed the transport and localization of EV1 and $\alpha2\beta1$ integrin in detail. During the first 5–15 min of internalization, the colocalization of $\alpha2\beta1$ integrin, clustered by sequential incubation with primary and secondary antibodies, with caveolin-1 was scarce but then increased gradually (Figure 1A). Similar results were obtained with caveolin-GFP and EV1 (Figure 1B). For comparison, clustering studies were performed in HeLa cells, which express endogenous levels of $\alpha2\beta1$ integrin. These cells also showed a low amount of colocalization between integrin and caveolin-GFP after 5 min but a higher amount of colocalization after 2 h (Figure 1B). Live imaging of expressed caveolin-GFP and clustered $\alpha2\beta1$ integrin for longer times revealed that colocalization between caveolin-1 and integrin increases still after 2 h (Supplemental Figure 1A).

Because SV40 is the best-characterized virus to use the caveolae pathway (Pelkmans *et al.*, 2001), we also used SV40 as a marker for caveolae pathway in our assay. SV40 accumulates with slow kinetics in caveosomes before continuing its journey to endoplasmic reticulum and nucleus (Pelkmans *et al.*, 2001). Because the step between caveosomes and endoplasmic reticulum is blocked by microtubule depolymerization, we used nocodazole to accumulate SV40 in caveosomes as described previously (Pietiäinen *et al.*, 2004). We treated the cells first with SV40-Alexa Fluor 568 (AF568) for 1.5 h at 37°C and then clustered $\alpha2\beta1$ integrin on the plasma membrane and allowed simultaneous internalization for further 5 min, 15 min, or 2 h. After 5 min, the colocalization between $\alpha2\beta1$ integrin and SV40-AF568 was still rather low (11.1% ± 1.4 SE; Figure 1C). However, after 15 min and 2 h, the colocalization had increased (17.1% ± 0.5 and 30.5% ± 4.5 SE, respectively), and it was evident in cytoplasmic accumulations (Figure 1C). Caveolin-1 labeling showed that after 2 h many of the vesicles containing SV40-AF568 and $\alpha2\beta1$ integrin were also positive for caveolin-1, suggesting that these structures were caveosomes. Quantification of colocalization between $\alpha2\beta1$ integrin and caveolin-1 in the same experiment showed very similar values (mean ± SE: 9.0 ± 2.8, 17.6 ± 1.4, and 29.2 ± 2.7% after 5 min, 15 min, and 2 h, respectively) as between integrin and SV40. Without integrin clustering the colocalization of SV40 with $\alpha2\beta1$ integrin was low (5.8 ± 0.6%; Figure 1C).

We then tested whether the pathway used by EV1 and $\alpha2\beta1$ integrin was associated with fluid uptake. For the purpose we used HRP and 10-kDa dextran as fluid-phase markers and found that they also accumulated in the structures positive for $\alpha2\beta1$ integrin (Figure 2A and Supplemental Figure 1B). EM studies indicated that most (>90%) integrin containing vesicles were positive for HRP after 5- and 15-min internalization (Figure 2A). After 5-min internalization, the structures were typically tubulovesicular (100% of the structures; ~200 structures calculated), but after 15 min, the structures had already changed to larger vesicular structures showing some internal vesicles (23% of the structures; ~200 structures calculated, Figure 2A). Confocal microscopy showed that also 10-kDa dextran internalized together with clustered integrin in both SAOS-$\alpha2\beta1$ and HeLa cells (Supplemental Figure 1B). To test whether integrin clustering had an effect on sorting of fluid-phase markers in SAOS-$\alpha2\beta1$ cells, we incubated the cells with lysine fixable 10-kDa dextran for 2 h (1-h pulse followed by 1-h chase) with or without integrin clustering (Figure 2B). If the cells were treated by integrin clustering, 30 ± 2% (mean ± SE) of dextran showed colocalization with caveolin-1–positive vesicles in the cytoplasm (Figure 2, B and C). Without integrin clustering, 14 ± 2% of internalized dextran showed colocalization with caveolin-1. We also tested whether integrin clustering affected the amount of dextran internalized to the cell (Supplemental Figure 1C). Quantification of the dextran signal after 1-h internalization showed no difference in the internalized amount of dextran with or without integrin clustering.

To verify that dextran was targeted to caveosomes due to integrin clustering, we tested whether dextran entered SV40-positive vesicles. Dextran was internalized for 2 h (1-h pulse followed by 1-h chase) in the presence of nocodazole and after SV40 pretreatment for 1.5 h. The results showed that after integrin clustering dextran was found in SV40-positive vesicles in the cytoplasm (Figure 2D) in a similar manner as dextran in caveolin-1–positive vesicles (Figure 2C). In contrast, without integrin clustering colocalization was lower (19 ± 2% [mean ± SE] without integrin clustering and 32 ±

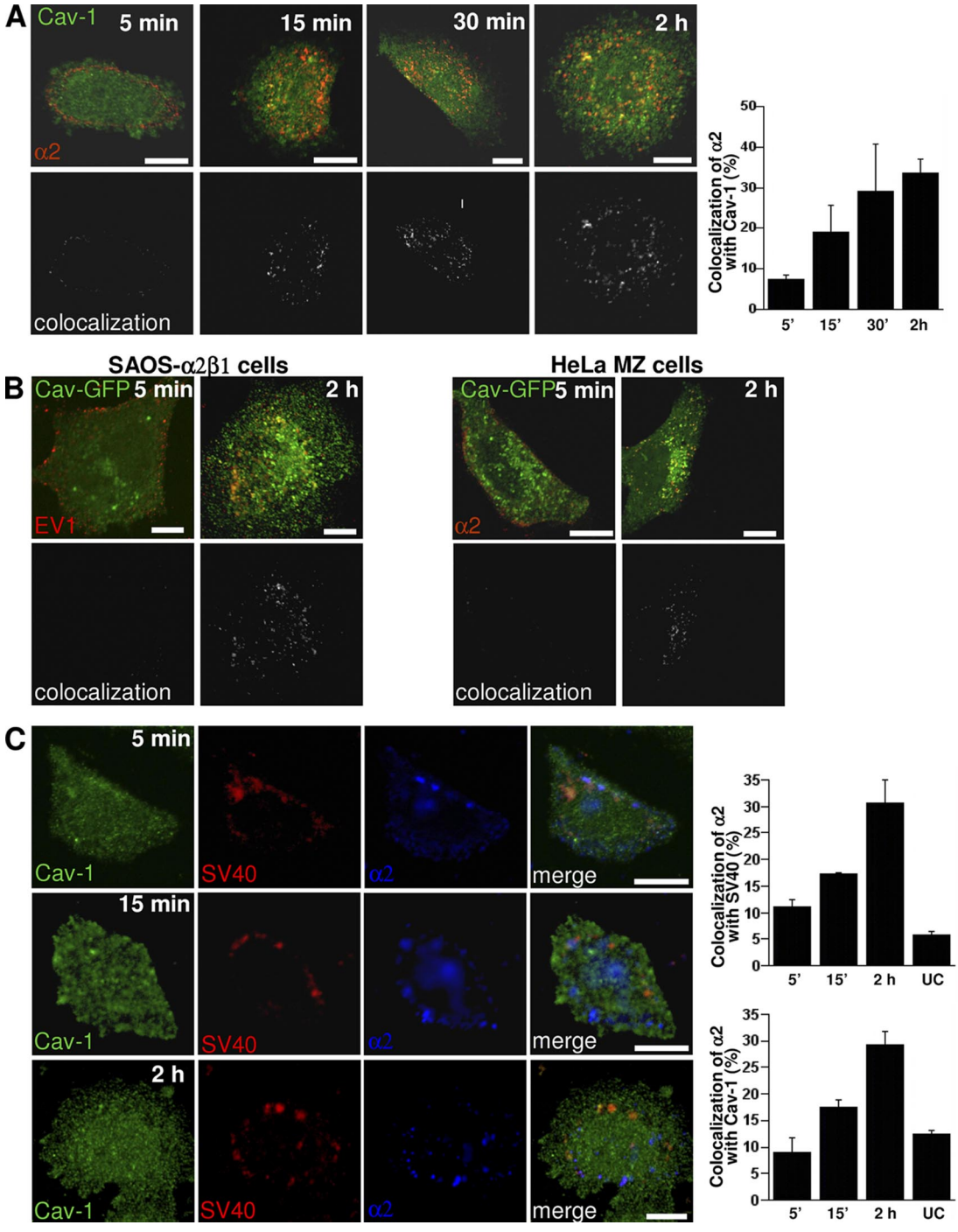

Figure 1. Clustered $\alpha 2\beta 1$ integrin and EV1 reach caveosomes from 30 min to 2 h. (A) Colocalization of the clustered $\alpha 2\beta 1$ integrin (red) with caveolin-1 (Cav-1) during integrin internalization (colocalizing voxels are presented as white). Colocalization was quantified from 30 cells from three independent experiments by using BioImageXD (see *Materials and Methods*). Bars, 10 μm. (B) Colocalization of EV1 or $\alpha 2\beta 1$ integrin ($\alpha 2$) with caveolin-1 was studied in HeLa MZ and SAOS-$\alpha 2\beta 1$ cells transfected with caveolin-GFP (Cav-GFP) at different time points after EV1 infection or integrin clustering. Labelings are shown as merge images (colocalizing voxels are presented as white). Bars, 10 μm. (C) SV40 was used as a marker for the caveolae pathway. SV40 accumulates with slow kinetics in caveosomes before continuing its journey to endoplasmic reticulum (ER) and nucleus. Nocodazole was used to depolymerize microtubules and block the step between caveosomes and ER to accumulate SV40 in caveosomes during 1.5-h preinternalization with SV40. Integrin $\alpha 2\beta 1$ ($\alpha 2$; blue) was then clustered and the colocalization between internalized $\alpha 2\beta 1$, SV40, and caveolin-1 was then followed for a further 5 min, 15 min, and 2 h. For the unclustered integrin control (UC) $\alpha 2\beta 1$ integrin was labeled after fixation. Colocalization was quantified as described in A. Bars, 10 μm.

2% after integrin clustering; Figure 2D). Interestingly, when we used the acid-sensitive dextran-FITC instead of dextran-Alexa 488 for this experiment, we found that the green signal was significantly lower (~80%) after internalization for 2 h without integrin clustering probably due to entry to an acidic environment (Supplemental Figure 1D). Instead,

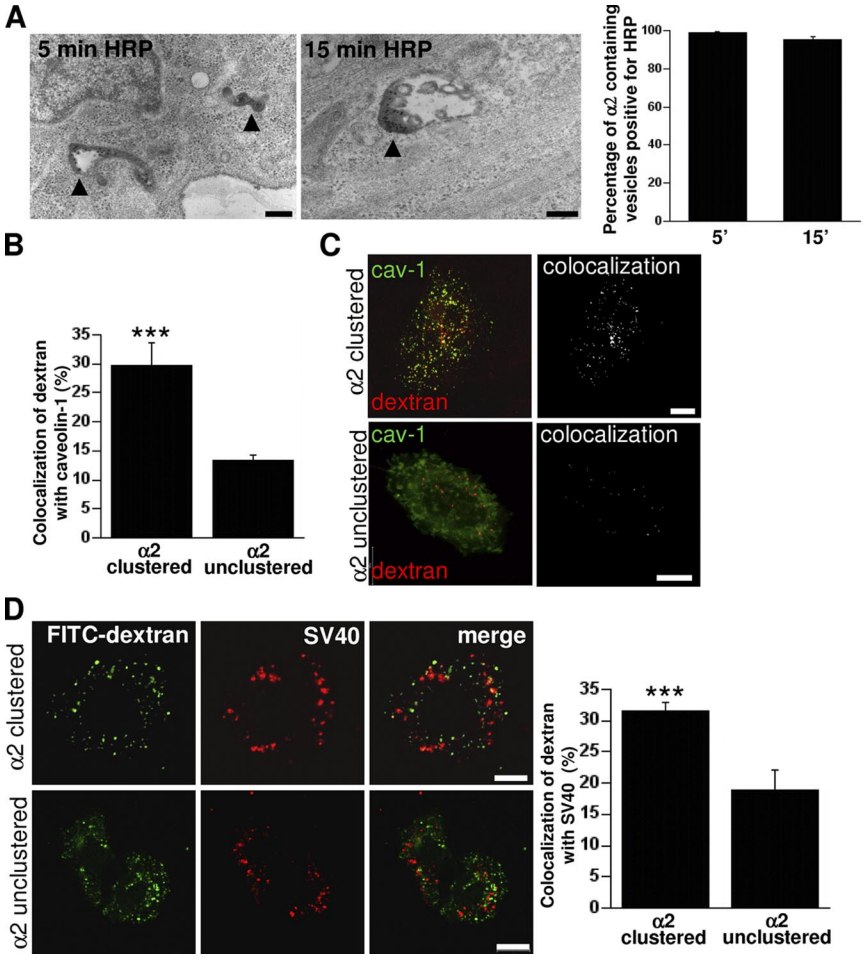

Figure 2. $\alpha 2\beta 1$ integrin clustering sorts fluid-phase cargo to caveosomes. (A) Clustered $\alpha 2\beta 1$ integrin was internalized for 5 and 15 min in the presence of 10 mg/ml HRP (left). Protein A gold (10 nm) shows the location of $\alpha 2\beta 1$ integrin in tubulovesicular and multivesicular structures colocalizing with HRP after 5 and 15 min, respectively (arrowheads). Percentage of $\alpha 2\beta 1$ integrin-positive endosomes ($\pm$SE) containing HRP was quantified from >200 structures. (B) Colocalization of lysine-fixable dextran (pulsed for 1 h and chased for 1 h) with caveolin-1. The assay was performed with ($\alpha 2$ clustered) or without ($\alpha 2$ unclustered) $\alpha 2\beta 1$ clustering, and colocalization was quantified as described in *Materials and Methods* by using BioImageXD (30 cells counted from three independent experiments). Examples of cells measured for this quantification are shown in C. Colocalized voxels are shown as white color (dextran Alexa 546, red; caveolin-1, green). (D) To verify that dextran was targeted to caveosomes due to integrin clustering, colocalization between dextran (1 mg/ml FITC-dextran) and internalized SV40 was measured (quantification of colocalization was from 30 cells from 3 independent experiments). Dextran was internalized for 2 h (1-h pulse followed by 1-h chase) in the presence of nocodazole and after SV40 pretreatment for 1.5 h. Bars, 200 nm (A), 10 μm (B–D).

after integrin clustering the cells showed bright green color, suggesting that those vesicles were not highly acidic.

These results together suggest that $\alpha 2\beta 1$ integrin, clustered by antibodies or EV1, is initially endocytosed to the cells together with fluid-phase markers and that integrin clustering causes routing of dextran to the caveosomal pathway instead of the default lysosomal pathway.

The Initial Entry of EV1 Is Dynamin and Caveolin Independent in SAOS-$\alpha 2\beta 1$ Cells

Because our results proposed that caveolin-1 is not involved in the earliest steps in EV1 and integrin entry, we tested the dynamin dependence of their internalization into SAOS-$\alpha 2\beta 1$ cells. Our earlier results in CV-1 cells suggested that in those cells EV1 infection was largely dependent on dynamin (Pietiäinen *et al.*, 2004). Surprisingly, the transfection of a dominant-negative (DN) dynamin 2 (K44A mutation) had no effect on EV1 infection in SAOS-$\alpha 2\beta 1$ cells (Figure 3A). Due to this difference to CV-1 cells, we tested the efficacy of the dynamin constructs with internalized transferrin. Calculations based on confocal microscopy sections showed that the dynamin K44A mutant inhibited transferrin entry by ~50% ($p < 0.001$; Figure 3B). Furthermore, clustered $\alpha 2\beta 1$ integrin could efficiently enter into SAOS-$\alpha 2\beta 1$ cells despite inhibition of dynamin function (Figure 3C). Unfortunately, we could not get a sufficient knockdown of dynamin with a SMARTpool siRNA to inhibit transferrin entry (data not shown). Similarly, we did not succeed in inhibiting transferrin entry using 80 μM Dynasore with 30- or 60-min preincubation in SAOS-$\alpha 2\beta 1$ cells (data not shown). Because the dynamin K44A construct could also only partially block the transferrin entry, the lack of dynamin dependence of EV1 infection and integrin internalization in SAOS-$\alpha 2\beta 1$ cells remains as a tentative conclusion.

We next tested a dominant-negative mutant of caveolin-3 (KSY), which efficiently inhibits SV40 infection (Roy *et al.*, 1999). Quantification of EV1 infection in transfected cells showed that the KSY mutant totally inhibited infection in SAOS-$\alpha 2\beta 1$ cells (Figure 3D). Differential labeling of the surface-bound and intracellular EV1 in transfected cells showed that EV1 was not arrested on the plasma membrane in any of the KSY-transfected cells. This assay was performed by labeling EV1 by using the same antibody before and after permeabilization with different colors (see *Materials and Methods*). Because the antibody added after permeabilization may still bind to EV1 on the plasma membrane due to polyclonal nature of the antibody, there is some overlap of the labels on the surface. However, the green color alone (added after permeabilization) shows the real internalized pixels in the fluorescent merge image. All observed cells transfected with the KSY mutant showed internalized EV1 (50 cells observed; Figure 3E). Confocal images showed that all EV1 internalization occurred similarly as after transfection with wild-type caveolin-3 construct (Figure 3E). Similarly, the internalization of $\alpha 2\beta 1$ integrin was not blocked by another dominant-negative mutant of caveo-

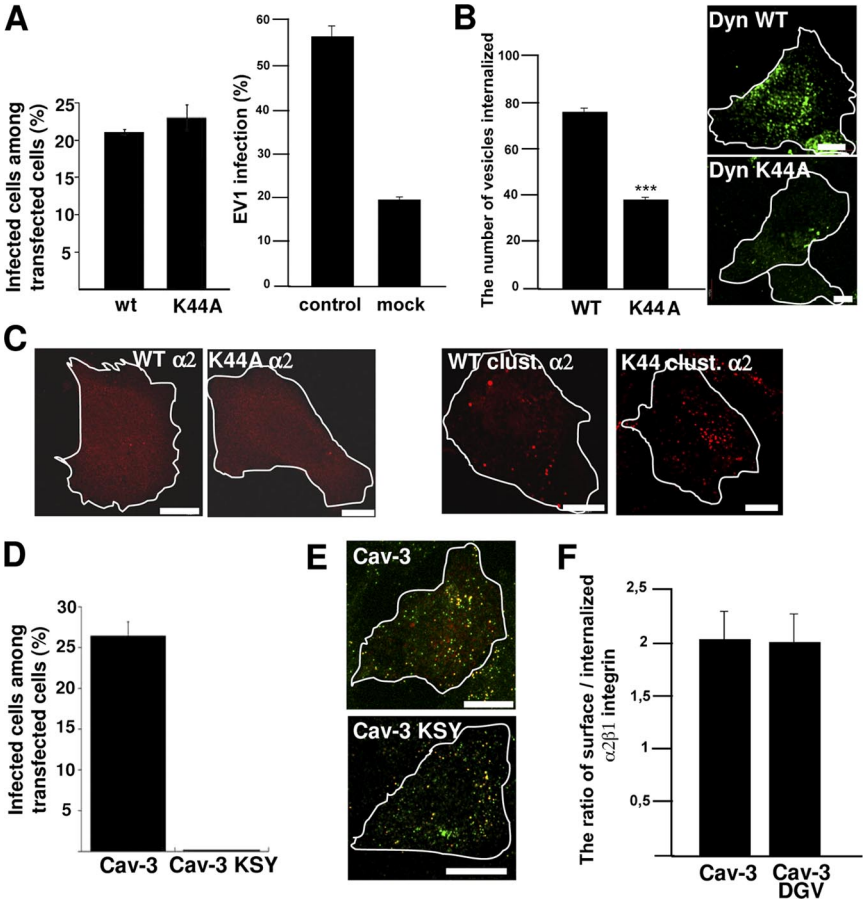

Figure 3. Early entry of EV1 and $\alpha 2\beta 1$ integrin is not dependent on dynamin 2 and caveolin in SAOS-$\alpha 2\beta 1$ cells. (A) The cells transfected with dynamin 2 constructs (wild-type, WT; DN dynamin 2, K44A) were analyzed for EV1 infection. For comparison, EV1 infection without transfection, and infection after mock transfection with yellow fluorescent protein (YFP) construct are shown. The results are mean values of three independent experiments (±SE). Transfection protocol causes a general decrease of EV1 infection (see also Figure 3B and 7B); therefore, the infectivity after transfection is always compared with the respective wild-type construct. (B) The inhibitory effect of transfected dynamin constructs on internalization of transferrin was quantified after 1-h internalization (60 cells from three experiments were quantified for the number of transferrin-containing vesicles by using a segmentation tool in BioimageXD; $p < 0.001$). Localization of transferrin-Alexa 488 after 1-h internalization is visualized in cells transfected with dynamin constructs. (C) Integrin $\alpha 2\beta 1$ (red), unclustered ($\alpha 2$), or clustered for 2 h (clust. $\alpha 2$) is shown in transfected cells. (D) DN mutant of caveolin-3 (Cav-3 KSY) and wild-type caveolin-3 (Cav-3) were transfected to the cells and their effects on EV1 infection was quantified. The result is a mean value of two independent experiments (±SE). (E) The effect of mutant (KSY) and wild-type caveolin-3 (Cav-3) on EV1 internalization was revealed by differential labeling of the surface-bound (red and colocalized red and green voxels) and intracellular EV1 (green alone) in transfected cells after 2-h internalization (see *Materials and Methods* for details). (F) The internalization of $\alpha 2\beta 1$ integrin in cells transfected with another DN mutant of caveolin-3 (DGV) or wild-type caveolin-3 was quantified using the internalization tool in BioimageXD. For the internalization, 30 cells from three experiments were counted for each case. Bars, 10 μm.

lin-3 (DGV; Figure 3F). We have shown earlier that this mutant has a significant, albeit milder, inhibitory effect on EV1 infection (Marjomäki *et al*., 2002).

Based on these results, we concluded that the initial entry of EV1 and $\alpha 2\beta 1$ integrin is independent of caveolin and dynamin in SAOS-$\alpha 2\beta 1$ cells. The results further suggest that the presence of caveolin-1 in the caveosomes may be important for EV1 infection.

$\alpha 2\beta 1$ Integrin Enters First Tubulovesicular Structures, Which Quickly Mature into Multivesicular Bodies

In the next series of experiments we tested marker proteins that have recently been linked to clathrin- and caveolin-independent fluid-phase pathways, namely, GPI-AP, CTxB, and flotillins. Our earlier results showed that before clustering on the plasma membrane, $\alpha 2\beta 1$ integrin resides on the raft areas positive for bacterial toxin aerolysin binding to GPI-AP (Upla *et al*., 2004). Here, we expressed the green fluorescent protein-tagged GPI-AP (GPI-GFP). Before the integrin internalization, the cells were treated with cycloheximide for 4 h to chase the GPI-GFP to the plasma membrane. Directly after clustering, at 0 min, integrin label showed small punctate labeling on the plasma membrane as a sign of cluster formation (Figure 4A), whereas unclustered integrin showed more diffuse staining (Supplemental Figure 2A). Confocal microscopy showed that after this rapid clustering on ice, GPI-GFP showed only a low amount of colocalization (5.5 ± 0.2% [mean ± SE]) with integrin, whereas without clustering the colocalization was relatively high on the plasma membrane (44.5 ± 1.6%; measured from 35 cells). After a short warm-up period, colocalization with GPI-GFP increased to some extent but stayed still rather low during the whole internalization period (Figure 4A). The colocalization of CTxB with clustered integrin was similarly low through the whole study period with a small peak after 30 min (Figure 4A). After 2 h, CTxB had already accumulated to a large extent in the perinuclear region, possibly in the Golgi or late endosomes (Figure 4A and Supplemental Figure 2A). We also tested the presence of flotillin 1 in these endosomes. From confocal sections, it was clear that flotillin 1 was not recruited to EV1-positive endosomes (Supplemental Figure 2B).

We tested the colocalization of internalized EV1 or integrin with EEA1, CI-MPR, and also CD63 (Supplemental Figure 3A). None of these classical endosomal markers showed colocalization with EV1 or integrin, suggesting that EV1 or $\alpha 2\beta 1$ integrin are not efficiently recruited to the conventional endosomes. Furthermore, live imaging of internalized integrin with a labeled LysoTracker showed no colocalization during a 3-h internalization period, suggesting that the integrin structures along the pathway are not highly acidified (Supplemental Figure 3B). However, this result does not rule out that integrin positive structures may become mildly acidic during internalization.

Next, we studied the nature of the cellular structures involved in early internalization at high resolution. We fol-

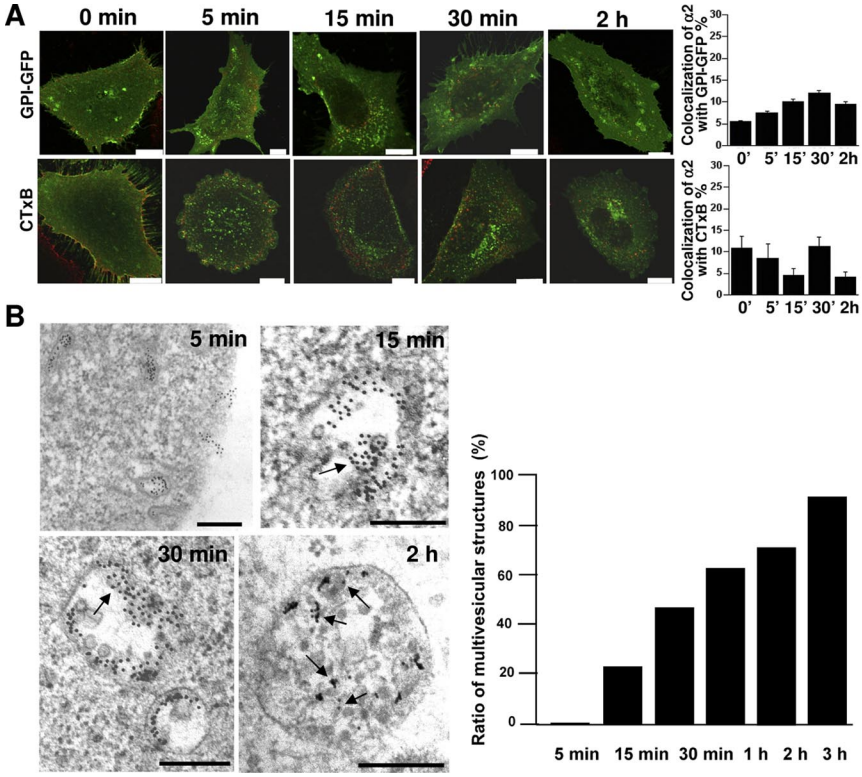

Figure 4. From the plasma membrane rafts $\alpha2\beta1$ integrin enters first simple tubulovesicular structures, which quickly mature to multivesicular bodies devoid of GPI-GFP and CTxB. (A) Expressed GPI-GFP (green; after 4-h cycloheximide treatment, 100 μg/ml) and exogenously added CTxB (green; 1 μg/ml) were internalized in the presence of clustered $\alpha2\beta1$ integrin (red) for different times. The colocalization of $\alpha2\beta1$ with these markers was quantified from 30 cells from three separate experiments by evaluating the number of colocalized voxels using BioImageXD. The results are expressed as percentages of $\alpha2\beta1$ voxels colocalizing with marker voxels (±SE). Bars, 10 μm. (B) $\alpha2\beta1$ integrin was treated on ice with a nonfunctional integrin antibody (HAS6), followed by a clustering secondary antibody and protein A gold (10 nm), and then internalized for different times at 37°C. Structures positive for $\alpha2\beta1$ integrin were classified for being tubulovesicular (see image for 5-min time point) or multivesicular structures (images between 15 min and 2 h). Together, 150–200 structures were calculated from different times. $\alpha2\beta1$ integrin associated with intraluminal membranes are pointed with arrows. The relative distribution of multivesicular structures of all integrin structures is plotted on the right. Bars, 200 nm.

lowed the routing of $\alpha2\beta1$ integrin clusters over time by EM using protein A gold binding to the secondary antibody, used in clustering of the integrin (Figure 4B). In parallel experiments, EV1 was also present to verify that they followed the same pathway as the clustered integrin (Supplemental Figure 4A). Calculations from those EM images showed that the structures positive for EV1 were also positive for internalized $\alpha2\beta1$ integrin (94 and 100% after 5 and 30 min, respectively; 20 cells and >100 positive structures were calculated), suggesting that they use the same endosomal structures during internalization. The EM samples with clustered integrin alone showed that 5–15 min after the clustering at 37°C some $\alpha2\beta1$ integrin was still present on the plasma membrane, but a large pool of $\alpha2\beta1$ integrins had entered the cell. Integrin $\alpha2\beta1$ was often found in smooth-surfaced vesicles and tubules that were clearly larger than caveolae and lacked the typical clathrin cage coating (Figure 4B). The mean size of these vesicles after 5-min internalization was 138 nm (SE 12 nm). After 15 min, a small fraction (23%) of the structures that were positive for integrin-linked gold particles showed more complex morphology: they were larger in size and showed internal vesicles (Figure 4B). The integrin was often present in the invaginations of the limiting membranes and in the internal vesicles (Figure 4B, arrows). Quantification of the number of integrin-positive structures showed that after 5 min the internalized integrins (100%) were in the tubulovesicular structures without internal vesicles, whereas after 2 h most of the integrins (72%) were in the complex multivesicular structures. The mean size of the structures after 2 h was 383 nm (SE 20 nm). This maturation process to multivesicular structures seemed to proceed further after 2 h because 1 h later, 92% of the structures were multivesicular.

The results suggest that EV1 and $\alpha2\beta1$ integrin first enter tubulovesicular structures that are early sorted away from raft-derived markers such as GPI-AP, CTxB, and flotillin 1. In addition, these structures mature into large multivesicular structures in the cytoplasm.

Inhibitors of the Na^+/H^+ Exchanger and Phospholipase C Inhibit EV1 Infection and Concomitantly Restrain the EV1/$\alpha2\beta1$ Integrin Entry Pathway

To test different regulators and markers associated with fluid-phase entry pathways, drugs such EIPA, an inhibitor of the amiloride-sensitive Na^+/H^+ exchanger (Meier *et al.*, 2002; Nakase *et al.*, 2004); LY294002, an inhibitor of phosphatidylinositol 3-kinase (PI3K); and U73122, an inhibitor of phosphatidylinositol-specific phospholipase C (PLC) (PI-PLC) (Veithen *et al.*, 1998; Amyere *et al.*, 2000) were used. We monitored their effects on dextran uptake in our experimental system and observed that in SAOS-$\alpha2\beta1$ cells, EIPA and U73122 blocked the dextran uptake to the periphery of the cells, whereas LY294002 caused only a minor effect on dextran uptake (Supplemental Figure 4B). In addition, we evaluated the cytotoxicity of these drugs using a commercial kit (Promega; see *Materials and Methods*), and we could verify that the cell viability was not affected during the experimental period (Supplemental Figure 4C).

We then tested whether EV1 infection and entry could be prevented by these pharmacological inhibitors (Figure 5). The drugs were added at different time points to analyze in more detail whether they were inhibiting the initial entry or also some later trafficking steps (Figure 5A). Control infection without any drug treatment showed that after 7 h (the total incubation time in the experiment), infectivity was ~70%. Measurement of the infectivity by confocal microscopy showed that EV1 infection was totally inhibited by EIPA and by U73122 and 70% with LY294002, when the drugs were administered 30 min before or directly after the virus binding (Figure 5A). When the drugs were administered to cells later (1–5 h post infection [p.i.]) it was clear that U73122 was an efficient blocker of infection only during the

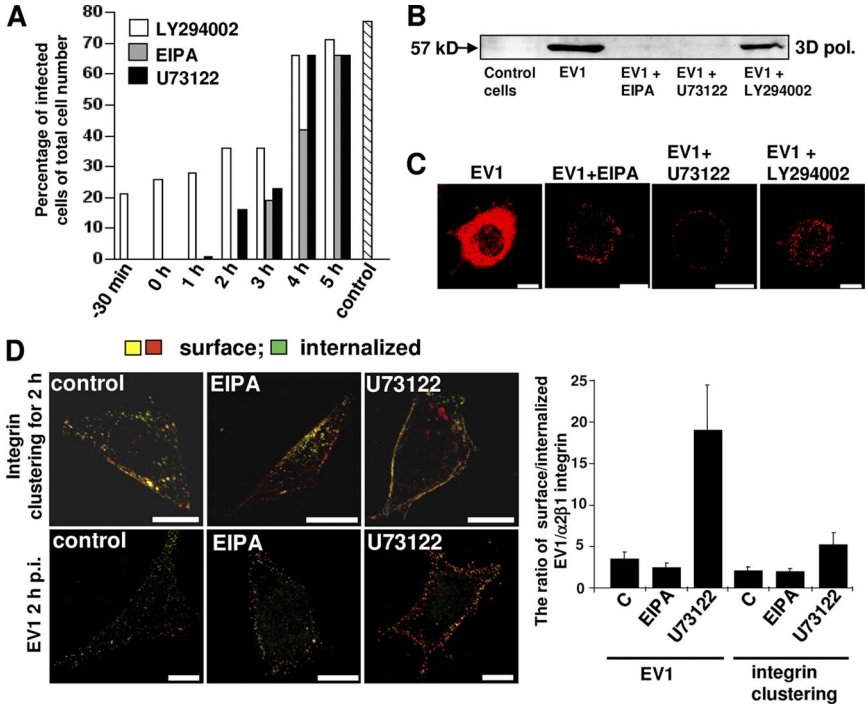

Figure 5. EV1 infection is blocked by macropinocytosis inhibitors. (A) EV1 was first bound on cells on ice, nonattached virus was washed away and receptor-bound virus was allowed to internalize at 37°C for 7 h in total. The drugs (EIPA, U73122, and LY294002) were added at different times during the infection. Infected cells were counted based on the emergence of new viral capsid proteins in the cytoplasm from fluorescent labeling. The results were counted from 150 to 200 cells for each case and the experiment was repeated once with similar results (control, infection without drugs). (B) Emergence of 3D polymerase as a proof of replication startup was visualized by SDS-PAGE and Western immunoblotting. Drugs were present during the whole 7-h period. (C) The localization of EV1 capsid proteins was visualized after different drug treatments 7 h p.i. Images are confocal sections through the central area of the cells. (D) Differential staining of the internalized and surface-bound $\alpha2\beta1$ integrin and EV1. Drugs were added 30 min before the assay, and they were present during the 2-h internalization period. EV1 or $\alpha2\beta1$ integrin were immunolabeled before and after permeabilization to reveal the surface-bound and intracellular proteins, respectively. The surface-bound proteins show both red and colocalized voxels (green and red together), whereas green alone represents the internalized proteins. The ratio of surface/internalized EV1 or $\alpha2\beta1$ integrin was determined using the internalization algorithm in BioImageXD software (see *Materials and Methods* for details). (Higher ratio means lower amount of internalization.) Bars, 10 μm.

early entry period. When this inhibitor was added 1 h p.i., some EV1-infected cells were detected, whereas EIPA completely blocked EV1 infection when added after 2 h p.i. The results of this infectivity titration also suggest that the viral genome is released around 2–3 h p.i. from the structures to start replication, which is in line with our previous results from real-time PCR measurements (Upla *et al*., 2008). The inhibitory effect of these drugs was also followed by the emergence of the 3D polymerase in the host cells marking the onset of viral replication (Figure 5B). Again, EIPA and U73122 totally inhibited the emergence of 3D polymerase, whereas LY294002 treatment inhibited but could not totally block the replication (Figure 5B).

We also wanted to visualize the cellular structures where EV1 accumulated after a treatment with the chemical inhibitors (Figure 5C). After 7 h in control condition, cells have had time to start the virus replication and the mass production of new viruses. Thus, the cytoplasm was full of newly synthesized EV1 capsid proteins in infected control cells. In contrast, the drug treatments blocked the viral infection as the incoming virus was blocked in vesicular structures or on the plasma membrane (Figure 5C). U73122 and EIPA caused accumulation of the virus close to the plasma membrane, whereas with LY294002 treatment, virus could enter membranous structures deeper in the cytoplasm.

To quantify the blocking effect of the inhibitors on internalization, we differentially labeled plasma membrane associated and internalized pools of EV1 and $\alpha2\beta1$ integrin (Figure 5C; see *Materials and Methods*). After 2 h, a large amount of EV1 or $\alpha2\beta1$ integrin was internalized into the cytoplasm in control cells. In U73122- and EIPA-treated cells, the virus and integrin remained close to the periphery (Figure 5D). We calculated the proportional amount of intracellular versus surface staining using the internalization algorithm of BioImageXD (Kankaanpää *et al*., 2006). In the assay, the surface signal for EV1 is comprised of the fluorescent signal added before permeabilization (red) and of the colocalized signal from the dye added after permeabilization (green). Thus, the green signal alone added after permeabilization (not colocalizing with the red) represents the true internalized voxels. In the case of clustered integrin, the labeling is done differently as the internalized dye (green) represents already the internalized signal. After fixation, the second dye (red) is added without permeabilization to label the surface signal. The quantification of this internalization showed that U73122 effectively inhibited the internalization of both EV1 and $\alpha2\beta1$ integrin (Figure 5D). In contrast, EIPA did no inhibit internalization per se but arrested further transport from the peripheral cytoplasm (Figure 5D).

Thus, our results show that these inhibitors that have recently been associated with fluid-phase endocytosis and macropinocytosis inhibited EV1 infection and blocked internalization of EV1 and $\alpha2\beta1$ integrin albeit at different stages and apparently by different mechanisms.

EIPA Prevents Maturation of Tubulovesicular Structures into Multivesicular Bodies and Inhibits Caveolin-1 Entry to These Structures

Because we discovered that the internalization of $\alpha2\beta1$ integrin and EV1 was affected by EIPA and U73122 at different stages, we wanted to study whether the targeting to the caveosomes was also altered. Without the inhibitors $\alpha2\beta1$ integrin accumulated efficiently in the multivesicular structures after 2- to 3-h internalization period (72 and 92%, correspondingly, Figures 2A, 4B, and 6A). U73122 treatment caused a total block of $\alpha2\beta1$ integrin transport on the plasma membrane (Figure 6A). EM images showed no integrin positive cytoplasmic structures in the cells treated with U73122. This verifies the results shown in Figure 5C, indicating a

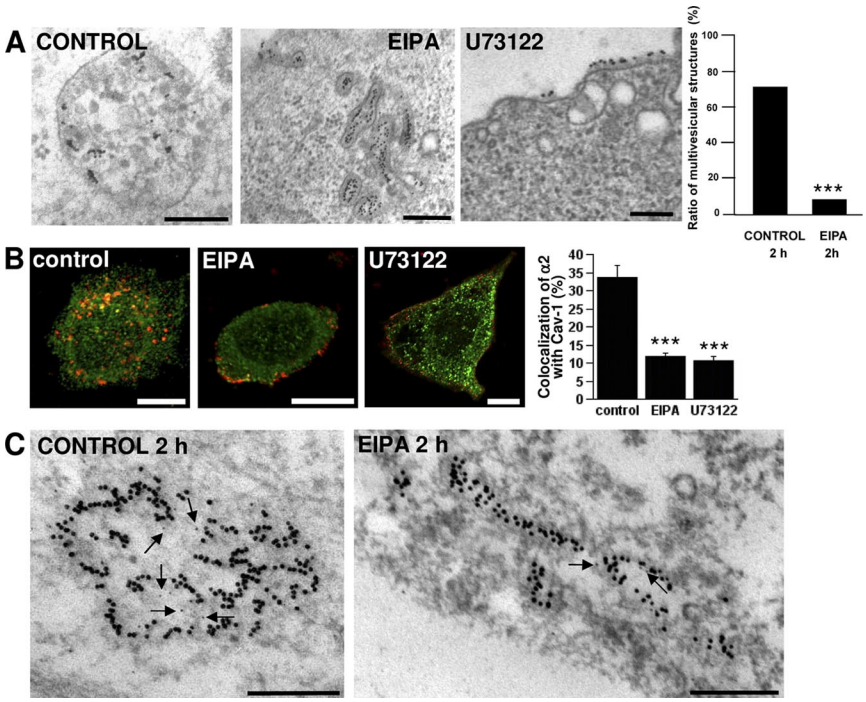

Figure 6. EIPA prevents maturation of tubulovesicular structures into multivesicular bodies and caveolin-1 entry to these structures. (A) EM images of internalized and clustered $\alpha2\beta1$ integrin after 2 h with EIPA or U73122 or without drugs (CONTROL). Bars, 200 nm. The proportional distribution of $\alpha2\beta1$ integrin in tubulovesicular versus multivesicular structures after EIPA treatment was counted from 150 to 200 structures. (B) Cells were labeled for caveolin-1 (green) and internalized $\alpha2\beta1$ integrin (red) after 2 h. Drugs were added 30 min before the experiment. Colocalization between internalized integrin and endogenous caveolin-1 was calculated from 30 cells for each case from three independent experiments. Bars, 10 μm. (C) Immuno-EM labeling of caveolin-1 (5-nm protein A gold) and $\alpha2\beta1$ integrin (10-nm protein A gold) after 2-h internalization in control cells or after EIPA treatment. Caveolin-1 was immunolabeled after fixation and permeabilization of the cells, whereas $\alpha2\beta1$ integrin was immunolabeled on the plasma membrane before internalization. Arrows indicate some of the caveolin-1 labels in the sections. Bars, 200 nm.

clear block at the level of the plasma membrane. In contrast, EIPA caused accumulation of $\alpha2\beta1$ integrin in tubulovesicular structures close to the cell periphery (Figure 6A). This is similar to the effect on virus/integrin uptake measured by fluorescence methods (Figure 5C). Quantification of the EM data showed that only 8% of the integrin-positive structures were multivesicular bodies after EIPA treatment even after 2 h. Additional ruthenium red staining in EM verified that the tubulovesicular structures after EIPA treatment for 2 h were truly intracellular and not connected to the plasma membrane ($p < 0.001$; Supplemental Figure 4D). After control internalization, 90 $\pm$ 5% of the vesicles were without ruthenium red stain and, similarly, after EIPA treatment 95 $\pm$ 2% of the structures were without ruthenium red stain. This suggests that EIPA allows early sorting into the simple tubulovesicular structures but prevents their further maturation into complex multivesicular structures.

Confocal microscopy and quantification of colocalization verified our earlier results that EV1 and $\alpha2\beta1$ integrin are targeted into caveolin-1–positive caveosomes during 2 h p.i. (Figure 6B) (Marjomäki *et al*., 2002; Pietiäinen *et al*., 2004; Upla *et al*., 2004). The PI-PLC inhibitor U73122 caused a clear block of integrin internalization on the plasma membrane and prevented colocalization with caveolin-1 in the cytoplasm ($p < 0.001$; Figure 6B). In the presence of EIPA, confocal images and quantification of colocalization showed that the vesicles positive for clustered $\alpha2\beta1$ integrin gained only a low amount of caveolin-1 during a 2-h incubation in the presence of the drug ($p < 0.001$; Figure 6B). We also performed immuno EM to see the caveolin-1 together with clustered integrin at higher resolution (Figure 6C). This double labeling showed the complex morphology and large size of integrin positive structures with caveolin-1 inside (Figure 6C). After the 2-h treatment with EIPA the peripheral tubular structures showed very low amount of caveolin-1 attached to the limiting membrane confirming our confocal microscopy results (Figure 6C).

These results showed that EIPA caused an enrichment of tubulovesicular structures in the cell periphery and prevented morphological maturation into multivesicular structures, concomitantly inhibiting caveolin-1 entry into these structures during the 2-h period.

Pak1 Regulates EV1 and α2β1 Integrin Entry

Paks are a group of serine/threonine kinases that were originally discovered as targets of Rho GTPases Rac and Cdc42 (Manser *et al*., 1994). Because Paks are also associated with fluid-phase endocytosis and macropinocytosis (Dharmawardhane *et al*., 2000), we wanted to study whether they also regulate EV1 and integrin entry. First, we tested the effects of the dominant-negative (Pak1 AID) and highly kinase active (Pak1 T423E) Pak1 constructs for dextran and transferrin uptake (Figure 7A). The Pak1 AID blocked dextran uptake efficiently on the plasma membrane, but it allowed normal entry of transferrin to the cells (Figure 7A). Quantification of this blocking effect showed that dextran entry was inhibited by 94% in Pak1 AID-transfected cells ($p < 0.001$). Furthermore, this construct also totally blocked EV1 infection, whereas after transfection with highly kinase active mutant (Pak1 T423E) or with wild-type Pak1 the infection was close to the values gained from mock plasmid transfection (N1-YFP; Figure 7B). Control infection without any transfection shows typically higher level of infection as the transfection protocol itself decreases infection. This phenomenon is not restricted to virus type used as we have encountered this with all tested viruses so far. Confocal microscopy after 2 h p.i. revealed that the Pak1 AID construct also clearly decreased the amount of EV1 in the cells (Figure 7C). After 6 h p.i. the cells transfected with Pak1 AID construct did not promote new viral protein synthesis, whereas other cells showed typically high amounts of newly synthesized capsid proteins (Figure 7C).

Because Paks are often regulated upstream by the Rho GTPases Rac1 and Cdc42, we tested their involvement in EV1 infection as well. We performed knockdown of Cdc42, Rac1, and RhoA, a Rho GTPase that does not activate Pak (Manser *et al*., 1994), by using siRNA and we studied EV1 infection in siRNA-transfected cells (Figure 8A). Despite the

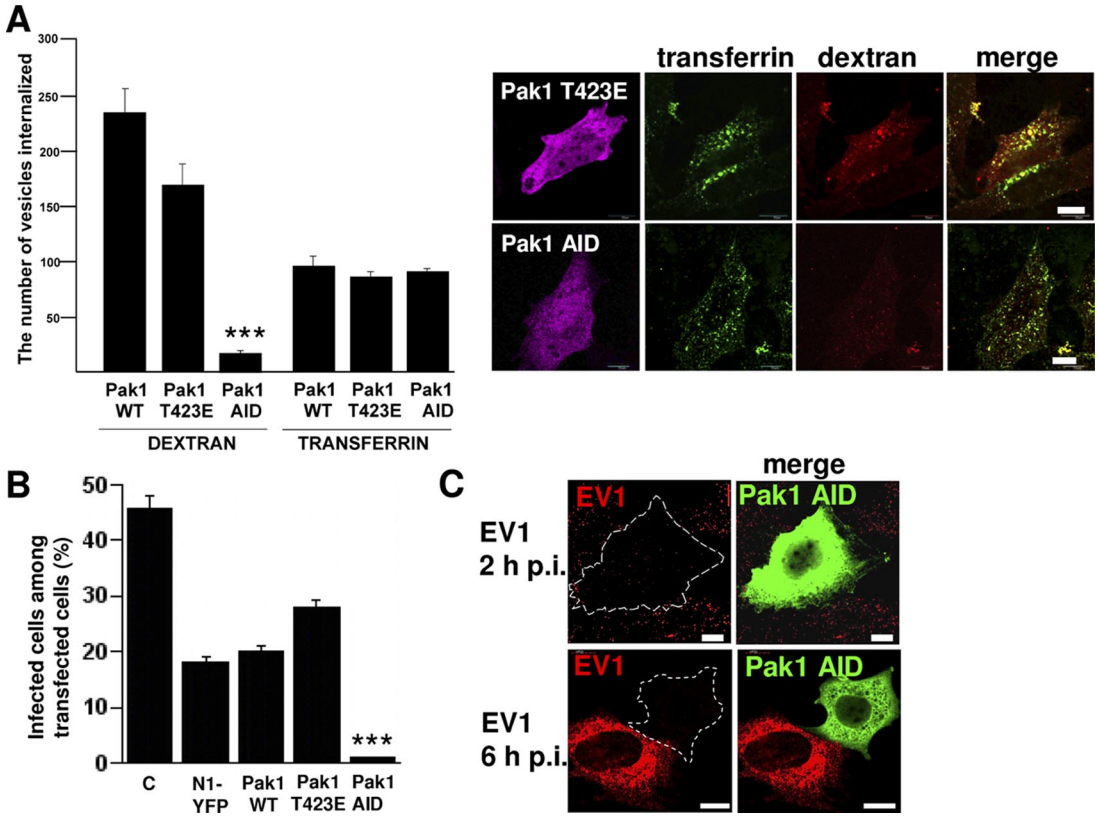

Figure 7. Pak1 regulates EV1/$\alpha 2\beta 1$ integrin entry. (A) The effects of WT, dominant-negative (Pak1 AID), and highly kinase active (Pak1 T423E) Pak1 constructs on internalization of dextran and transferrin. Quantification of internalized dextran and transferrin is shown as the amount of internalized vesicles positive for the tracer, determined by the segmentation tool in BioimageXD. The quantification was done from 30 cells from three independent experiments (***$p < 0.001$) Confocal images show the expressed construct (magenta), internalized transferrin (green; 0.25 mg/ml transferrin Alexa 488) and dextran (red; 0.25 mg/ml rhodamine dextran) in cells transfected with Pak1 T423E and Pak1 AID. (B) Pak1 constructs were tested for their effect on EV1 infection. The result is a mean value of three independent experiments (±SE). Control infection without transfection (C), and infection after mock transfection (N1-YFP) is shown. (C) Confocal images after 2 h and 6 h p.i. show very low amount of virus (red) in the transfected cells (marked as dotted line; in merged images Pak1 transfected cells are labeled as green). Bars, 10 μm.

efficient knockdown of Cdc42 (92% drop in protein expression), it showed very little effect in EV1 infection (Figure 8A). siRNA against RhoA showed a 64% knockdown of RhoA protein level, but we did not observe any effect on EV1 infectivity. Rac1 (63% knockdown of Rac1 expression) had a stronger and statistically significant inhibitory effect on EV1 infection suggesting that it may be involved in Pak1 regulation. Evaluation of the siRNA effects on dextran and transferrin endocytosis showed that Rac1 inhibited dextran entry in 75% of the siGLO-positive cells (marking efficient transfection of the siRNA), but it had no effect on transferrin entry (data not shown).

We wanted to verify the effects of Cdc42, Rac1, and RhoA using their wild-type and dominant-negative constructs. Similar to the siRNA experiment, transfection of dominant-negative constructs for Cdc42 and RhoA had no effect on EV1 infection compared with the respective wild-type constructs (Figure 8B). In contrast, as the siRNA already suggested, the dominant-negative construct of Rac1 caused a clear inhibition of EV1 infection.

Because Paks and RhoGTPases are known regulators of actin dynamics, we decided to monitor the appearance of actin filaments in more detail (Figure 8C). In control SAOS-$\alpha 2\beta 1$ cells actin was located in stress fibers and in the cortical actin meshwork (Figure 8C). Actin labeling also colocalized with Pak1 in stress fibers in control cells. After 5-min incubation with EV1, the stress fibers were, to a large extent, depolymerized (in 46% of all the cells; Figure 8C). The stress fibers reappeared in later time points (Figure 8, C and D). Strikingly, 5 min p.i., and coinciding with actin depolymerization, Pak1 showed extensive accumulation in the nucleus and some colocalization with depolymerized actin in the cytoplasm. After 2 h, Pak1 had relocated to the cytoplasm but was still found close to the nucleus.

We wanted to verify the effect of Pak1 by using specific antibodies against the activated phospho Pak1. Fluorescent imaging of phosho-Pak1 showed that, after overnight starvation, the level of phospho-Pak1 was low in the cells but increased already during 5 min of EV1 entry ($p < 0.01$; Figure 8D and Supplemental Figure 5A). Quantification of 20 cells in each time point revealed that phospho-Pak1 was even more active after 15–30 min p.i. ($p < 0.001$). Active Pak1 was still observed after 2 h p.i., but the signal was already lower than after 15–30 min p.i. (Supplemental Figure 5A).

We also monitored the direct effects of actin polymerizing and stabilizing drugs on viral infection (Supplemental Figure 5B). Depolymerizing drugs such as cytochalasin D partly inhibited EV1 infection when the cells were preincubated with the drug for 30 min. However, by increasing the preincubation time the infection was concomitantly blocked. The stabilizing drug (jasplakinolide) inhibited EV1 infection

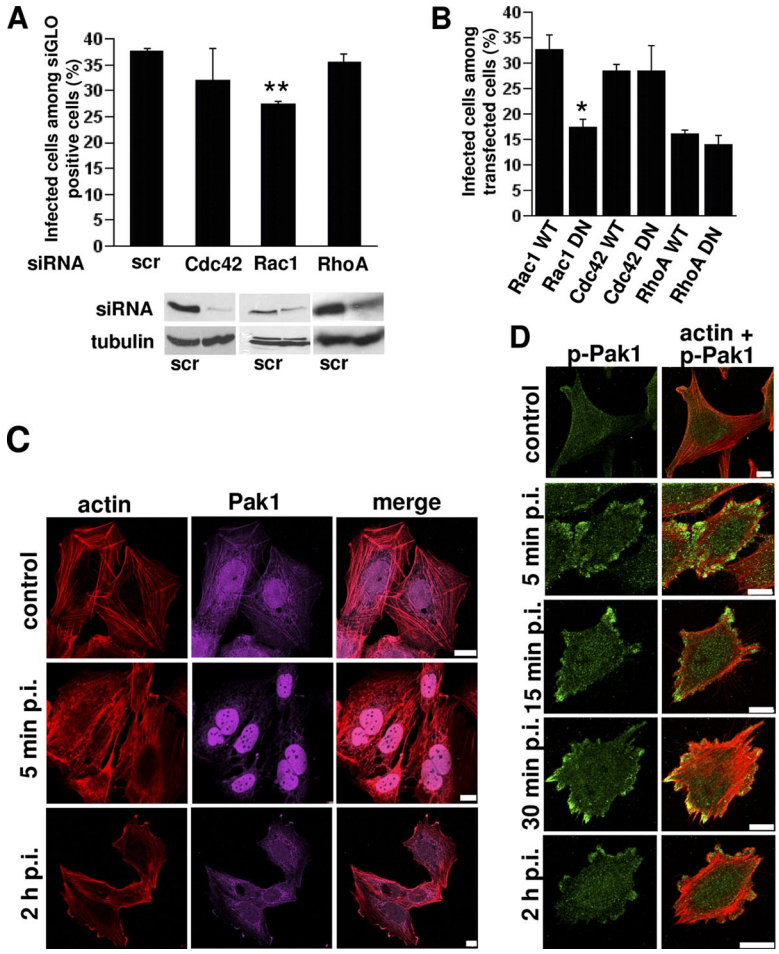

Figure 8. EV1 infection is regulated by Rac1 and actin dynamics. (A) RhoGTPases Cdc42, Rac1 and RhoA were knocked down using specific siRNA or control siRNA (scr) in the presence of a siGLO transfection marker. EV1 infection was quantified in these cells 6 h p.i. The result is a mean value of two independent experiments (±SE). Together, 300–400 siGLO–positive cells were counted for each construct. The knockdown effect was verified by Western blotting using tubulin as loading control. (B) The effects of Rac1, Cdc42, and RhoA were also verified by EV1 infection assay in cells transfected with WT and DN constructs. The result is a mean value of three independent experiments (±SE). (C) Pak1 (magenta) and actin (TRITC-phalloidin; red) were visualized after EV1 infection for 5 min and 2 h p.i. Bars, 10 μm. (D) Phospho Pak1 (green) was immunolabeled and actin (TRITC-phalloidin; red) was visualized after starvation (control) and EV1 treatment of SAOS-$\alpha2\beta1$ cells for different times (between 5 min and 2 h). Bars, 10 μm.

very efficiently even after a short preincubation period (Supplemental Figure 5, B and C). Confocal microscopy showed that the depolymerizing drugs caused accumulation of EV1 at the periphery of the cells, but jasplakinolide treatment caused a total block of EV1 transport from the plasma membrane (data not shown).

The results suggest that Pak1 regulates EV1 entry and infection and is itself activated very early coincident with rapid actin depolymerization. Furthermore, the results suggest that the Rho GTPase Rac1 regulates EV1 infection and may be the upstream regulator of Pak1.

DISCUSSION

We have studied the cell entry pathway of a human picornavirus, EV1, as a model system to understand events that occur during integrin-dependent uptake of cargo (Marjomäki *et al*., 2002; Pietiäinen *et al*., 2004; Upla *et al*., 2004; Xing *et al*., 2004). Our earlier biochemical and imaging studies have shown that EV1 is internalized in complex with its receptor, $\alpha2\beta1$ integrin, and further targeted into caveosomes.

This study showed that EV1 reaches the caveolin-1–positive compartment only after 15 min, suggesting that an entry pathway other than caveolae is mainly used during the first minutes of internalization. The recruitment of caveolin-1 or SV40 to integrin-positive endosomes was a gradual process, suggesting that the integrin-containing vesicles fused with internalized caveolae or caveosomal vesicles in the cytoplasm. A striking feature, associated with $\alpha2\beta1$ integrin clustering, was the sorting of fluid-phase markers into caveosomes. Without integrin clustering, internalized dextran was not found in caveosomes but rather seemed to be sorted to the default pathway, to the acidic endosomes of the clathrin pathway. The results thus suggest that this pathway is triggered after integrin clustering.

EM studies showed the emergence of tubulovesicular endosomes in the cell periphery after $\alpha2\beta1$ integrin clustering. The raft-derived GPI-AP is also endocytosed into tubulovesicular structures that have recently been termed GPI-anchor enriched early endosomal compartments (GEECs) (Sabharanjak *et al*., 2002; Kirkham and Parton, 2005). After internalizing via GEECs, GPI-AP is efficiently sorted into recycling early endosomes or early endosomes en route to late endosomes, depending on the cell type (Fivaz *et al*., 2002; Sabharanjak *et al*., 2002; Kalia *et al*., 2006). Our results showed that clustered $\alpha2\beta1$ integrin did not enter GEECs nor to any structures of the clathrin pathway, together suggesting that there is no overlap with the pathway used by GPI-AP. CTxB showed a small peak of colocalization after 30-min internalization, possibly representing colocalization in caveosomal structures on its way to the Golgi. Flotillins 1 and -2 have recently been shown to define their own pathway to the cytoplasm (Glebov *et al*., 2006). Here, confocal microscopy showed that flotillin 1 was not recruited on integrin-related endosomes, suggesting that integrin pathway differed also from the flotillin pathway.

EV1 infection and uptake of $\alpha 2\beta 1$ integrin were not apparently regulated by dynamin 2 in SAOS-$\alpha 2\beta 1$ cells in contrast to previous results obtained using the CV-1 cell line (Pietiäinen *et al*., 2004). The lack of dynamin dependence in SAOS-$\alpha 2\beta 1$ cells was suggested based on the lack of effect by the expressed DN dynamin 2 constructs. The mutant K44A dynamin inhibited the transferrin entry by 50%, in contrast to SMARTpool dynamin siRNA or Dynasor tested in SAOS-$\alpha 2\beta 1$ cells, which showed no effect on transferrin entry. Due to the moderate effect on transferrin uptake, however, the lack of dynamin dependence remains as a conclusion. The difference of dynamin dependence between CV-1 cells and that of SAOS-$\alpha 2\beta 1$ cells may be linked to other observed differences in the overall uptake in these cells. Namely, in our previous study, we found that the stabilizing drug jasplakinolide had no effect for EV1 infection in CV-1 cells (Pietiäinen *et al*., 2004) in contrast to the opposite results from SAOS-$\alpha 2\beta 1$ cells here. Interestingly, our recent results showed that in SAOS-$\alpha 2\beta 1$ cells EV1 and integrin entry are regulated by the carboxy-terminal binding protein 1/brefeldin A-ribosylated substrate (CtBP1/BARS; Liberali *et al*., 2008), which has been shown to regulate dynamin-independent entry in some cell lines (Bonazzi *et al*., 2005).

The endosomes containing clustered integrin went through a maturation process from tubulovesicular endosomes into more complex multivesicular structures. This maturation started 15 min p.i. and continued for 3 h. Recently, the epidermal growth factor (EGF) receptor was shown to enter smooth-surfaced vesicles that went through a rapid maturation into multivesicular bodies lacking markers of the classical late endosomes (White *et al*., 2006). Integrin-positive multivesicular structures were also reminiscent of membranous caveolin-1–enriched structures containing transforming growth factor-β receptor (Di Guglielmo *et al*., 2003). Recent data suggest that also SV40 may be found in multivesicular structures in CV-1 cells (Ari Helenius, personal communication), further suggesting that multivesicular structures may be associated with the caveolae pathway. Interestingly, EIPA blocked this morphological maturation, with a concomitant block in EV1 infection. Whether this block is directly linked to morphological maturation or some other effect remains to be studied.

While looking for factors that regulate entry of EV1 and $\alpha 2\beta 1$ integrin, it became clear that most of them have recently been associated with macropinocytosis. Macropinocytosis may be elicited by phorbol myristate acetate (PMA) and growth factors such as EGF (Racoosin and Swanson, 1992). We have previously shown that EV1 infection and integrin clustering activate PKCα to a similar extent as PMA treatment and this activity is also needed for EV1 internalization (Upla *et al*., 2004). In addition to PKC activity (Grimmer *et al*., 2002), macropinocytosis is suggested to depend on Rac1 (Ridley *et al*., 1992), Pak1 (Manser *et al*., 1997), PLC (Amyere *et al*., 2000), PI3K (Amyere *et al*., 2000), and recently also CtBP1/BARS (Liberali *et al*., 2008). Treatment with EIPA (Liu *et al*., 2002; Wadia *et al*., 2004) and inhibition of PI-PLC, PI3K, Rac1, and especially Pak1, all had an effect on EV1 infection and integrin internalization, suggesting that many of the players in entry are shared with macropinocytosis. Our recent results showing that CtBP1/BARS regulates EV1 and integrin entry (Liberali *et al*., 2008) further confirm that conclusion.

Inhibition of Pak1 by overexpressing the AID domain caused a block of fluid-phase and EV1 entry, probably by inhibiting the depolymerization of actin filaments as has been shown for the AID mutant previously (Papakonstanti and Stournaras, 2002). After activation, e.g., by EGF, Pak1 has been shown to accumulate in the nucleus (Singh *et al*., 2005). Similarly, EV1 treatment caused a rapid nuclear localization of Pak1 suggesting that it is indeed activated very early during EV1 infection. This further confirms that Pak1 is a crucial kinase regulating EV1/integrin internalization. Paks regulate the actin–myosin cytoskeleton and have been shown to be downstream targets of Cdc42 and Rac1 (Manser *et al*., 1997; Dharmawardhane *et al*., 2000). Inhibition of Rac1 and the concomitant inhibition of EV1 infection suggest that Rac1 is involved in the regulation of EV1/$\alpha 2\beta 1$ integrin entry and possibly in Pak1 activation.

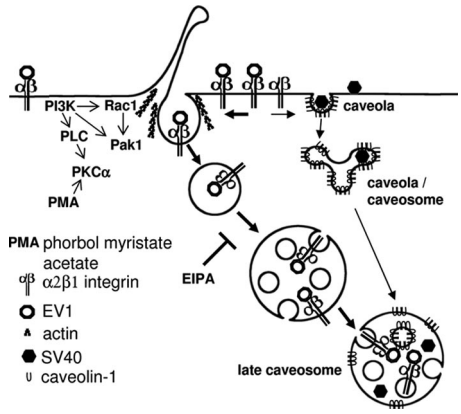

Figure 9. The proposed model for entry of EV1 and clustered $\alpha 2\beta 1$ integrin into cell. Internalized tubulovesicular structures mature into multivesicular bodies, and they are able to fuse with internalized caveolae or caveosomal structures containing caveolin-1 and SV40. The resulting fused structures may be considered as late caveosomes.

Majority of the data suggest that clathrin- and caveolin-independent carriers fuse with classical endosomes, preferably early or recycling early endosomes (Kirkham and Parton, 2005; Kalia *et al*., 2006; Marsh and Helenius, 2006; Mettlen *et al*., 2006; Mayor and Pagano, 2007). Putative fusion with caveosomes has been suggested as one alternative (Marsh and Helenius, 2006). $\alpha 2\beta 1$ integrin and EV1 showed colocalization with caveosomal markers but no apparent colocalization with markers of early endosomes, recycling early endosomes, or late endosomes/lysosomes, or accumulation in acidic structures along their entry route, suggesting that there is no clear connection to the clathrin-dependent pathway.

We propose that $\alpha 2\beta 1$ integrin clustering triggers a novel sorting pathway to caveosomes (Figure 9). In our model, the initial uptake is independent of clathrin and caveolin, and dynamin in some cell types, but occurs together with fluid-phase markers to peripheral tubulovesicular endosomes. Transient actin depolymerization is needed for successful entry and the process is blocked by inhibitors of PI-PLC, PI3K, and PKC, regulated by Pak1 and Rac1, and inhibited by EIPA. GPI-AP, CTxB, and flotillin 1 do not follow integrin and EV1 to the intracellular endosomes. These vesicles undergo maturation into multivesicular structures that are able to fuse with internalized caveolae or caveosomal structures containing caveolin-1 and SV40. The resulting fused structures may be considered as late caveosomes.

ACKNOWLEDGMENTS

We thank Arja Mansikkaviita, Raija Vassinen, Soile Huotari, and Paavo Niutanen for technical assistance and Dr. Daniel J. White for revising the language. We thank Drs. Antonino Colanzi, Alberto Luini, and Jari Ylänne for

critical reading of the manuscript and Drs. Ari Helenius, Jean Gruenberg, and Lucas Pelkmans for helpful discussions. This work was supported by grants from the Academy of Finland and the National graduate school on nanoscience. P.L. is a fellow of the Italian Foundation for Cancer Research (Fondazione Italiana Ricerca Cancro, Milan, Italy).

REFERENCES

Amyere, M., Payrastre, B., Krause, U., Van Der Smissen, P., Veithen, A., and Courtoy, P. J. (2000). Constitutive macropinocytosis in oncogene-transformed fibroblasts depends on sequential permanent activation of phosphoinositide 3-kinase and phospholipase C. Mol. Biol. Cell *11*, 3453–3467.

Auvinen, P., Mäkelä, M. J., Roivainen, M., Kallajoki, M., Vainionpää, R., and Hyypiä, T. (1993). Mapping of antigenic sites of coxsackievirus B3 by synthetic peptides. APMIS *101*, 517–528.

Bonazzi, M. *et al*. (2005). CtBP3/BARS drives membrane fission in dynamin-independent transport pathways. Nat. Cell. Biol. *7*, 570–580.

Conner, S. D., and Schmid, S. L. (2003). Regulated portals of entry into the cell. Nature *422*, 37–44.

Costes, S. V., Daelemans, D., Cho, E. H., Dobbin, Z., Pavlakis, G., and Lockett, S. (2004). Automatic and quantitative measurement of protein-protein colocalization in live cells. Biophys. J. *86*, 3993–4003.

Dharmawardhane, S., Schurmann, A., Sells, M. A., Chernoff, J., Schmid, S. L., and Bokoch, G. M. (2000). Regulation of macropinocytosis by p21-activated kinase-1. Mol. Biol. Cell *11*, 3341–3352.

Di Guglielmo, G. M., Le Roy, C., Goodfellow, A. F., and Wrana, J. L. (2003). Distinct endocytic pathways regulate TGF-beta receptor signalling and turnover. Nat. Cell. Biol. *5*, 410–421.

Fivaz, M., Vilbois, F., Thurnheer, S., Pasquali, C., Abrami, L., Bickel, P. E., Parton, R. G., and van der Goot, F. G. (2002). Differential sorting and fate of endocytosed GPI-anchored proteins. EMBO J. *21*, 3989–4000.

Glebov, O. O., Bright, N. A., and Nichols, B. J. (2006). Flotillin-1 defines a clathrin-independent endocytic pathway in mammalian cells. Nat. Cell. Biol. *8*, 46–54.

Grimmer, S., van Deurs, B., and Sandvig, K. (2002). Membrane ruffling and macropinocytosis in A431 cells require cholesterol. J. Cell Sci. *115*, 2953–2962.

Ivaska, J., Reunanen, H., Westermarck, J., Koivisto, L., Kähäri, V. M., and Heino, J. (1999). Integrin alpha2beta1 mediates isoform-specific activation of p38 and upregulation of collagen gene transcription by a mechanism involving the alpha2 cytoplasmic tail. J. Cell Biol. *147*, 401–416.

Kalia, M., Kumari, S., Chadda, R., Hill, M. M., Parton, R. G., and Mayor, S. (2006). Arf6-independent GPI-anchored protein-enriched early endosomal compartments fuse with sorting endosomes via a Rab5/phosphatidylinositol-3′-kinase-dependent machinery. Mol. Biol. Cell *17*, 3689–3704.

Kankaanpää, P., Pahajoki, K., Marjomäki, V., Heino, J., White, D., and BioImage, X. D. (2006) BioImageXD–free open source software for analysis and visualization of multidimensional biomedical images. (http://www.bioimagexd.net).

Kirkham, M., and Parton, R. G. (2005). Clathrin-independent endocytosis: new insights into caveolae and non-caveolar lipid raft carriers. Biochim. Biophys. Acta *1745*, 273–286. [correction published in Biochim Biophys Acta (2005). *1746*, 349–363].

Liberali, P. *et al*. (2008). The closure of Pak1-dependent macropinosomes requires the phosphorylation of CtBP1/BARS. EMBO J. *27*, 970–981.

Liu, N. Q. *et al*. (2002). Human immunodeficiency virus type 1 enters brain microvascular endothelia by macropinocytosis dependent on lipid rafts and the mitogen-activated protein kinase signaling pathway. J. Virol. *76*, 6689–6700.

Manser, E., Huang, H. Y., Loo, T. H., Chen, X. Q., Dong, J. M., Leung, T., and Lim, L. (1997). Expression of constitutively active alpha-PAK reveals effects of the kinase on actin and focal complexes. Mol. Cell. Biol. *17*, 1129–1143.

Manser, E., Leung, T., Salihuddin, H., Zhao, Z. S., and Lim, L. (1994). A brain serine/threonine protein kinase activated by Cdc42 and Rac1. Nature *367*, 40–46.

Marjomäki, V. S., Huovila, A. P., Surkka, M. A., Jokinen, I., and Salminen, A. (1990). Lysosomal trafficking in rat cardiac myocytes. J. Histochem. Cytochem. *38*, 1155–1164.

Marjomäki, V., Pietiäinen, V., Matilainen, H., Upla, P., Ivaska, J., Nissinen, L., Reunanen, H., Huttunen, P., Hyypiä, T., and Heino, J. (2002). Internalization of echovirus 1 in caveolae. J. Virol. *76*, 1856–1865.

Marjomäki, V., and Schaible, U. E. (2005). Microbial strategies to exploit host cells. EMBO Rep. *6*, 408–412.

Marsh, M., and Helenius, A. (2006). Virus entry: open sesame. Cell *124*, 729–740.

Mayor, S., and Pagano, R. E. (2007). Pathways of clathrin-independent endocytosis. Nat. Rev. Mol. Cell Biol. *8*, 603–612.

Meier, O., Boucke, K., Hammer, S. V., Keller, S., Stidwill, R. P., Hemmi, S., and Greber, U. F. (2002). Adenovirus triggers macropinocytosis and endosomal leakage together with its clathrin-mediated uptake. J. Cell Biol. *158*, 1119–1131.

Mettlen, M., Platek, A., Van Der Smissen, P., Carpentier, S., Amyere, M., Lanzetti, L., de Diesbach, P., Tyteca, D., and Courtoy, P. J. (2006). Src triggers circular ruffling and macropinocytosis at the apical surface of polarized MDCK cells. Traffic *7*, 589–603.

Nakase, I. *et al*. (2004). Cellular uptake of arginine-rich peptides: roles for macropinocytosis and actin rearrangement. Mol. Ther. *10*, 1011–1022.

Papakonstanti, E. A., and Stournaras, C. (2002). Association of PI-3 kinase with PAK1 leads to actin phosphorylation and cytoskeletal reorganization. Mol. Biol. Cell *13*, 2946–2962.

Pelkmans, L., Kartenbeck, J., and Helenius, A. (2001). Caveolar endocytosis of simian virus 40 reveals a new two-step vesicular-transport pathway to the ER. Nat. Cell Biol. *3*, 473–483.

Pietiäinen, V., Marjomäki, V., Upla, P., Pelkmans, L., Helenius, A., and Hyypiä, T. (2004). Echovirus 1 endocytosis into caveosomes requires lipid rafts, dynamin II, and signaling events. Mol. Biol. Cell *15*, 4911–4925.

Racoosin, E. L., and Swanson, J. A. (1992). M-CSF-induced macropinocytosis increases solute endocytosis but not receptor-mediated endocytosis in mouse macrophages. J. Cell Sci. *102*, 867–880.

Ridley, A. J., Paterson, H. F., Johnston, C. L., Diekmann, D., and Hall, A. (1992). The small GTP-binding protein rac regulates growth factor-induced membrane ruffling. Cell *70*, 401–410.

Roy, S., Luetterforst, R., Harding, A., Apolloni, A., Etheridge, M., Stang, E., Rolls, B., Hancock, J. F., and Parton, R. G. (1999). Dominant-negative caveolin inhibits H-Ras function by disrupting cholesterol-rich plasma membrane domains. Nat. Cell Biol. *1*, 98–105.

Sabharanjak, S., Sharma, P., Parton, R. G., and Mayor, S. (2002). GPI-anchored proteins are delivered to recycling endosomes via a distinct cdc42-regulated, clathrin-independent pinocytic pathway. Dev. Cell *2*, 411–423.

Singh, R. R., Song, C., Yang, Z., and Kumar, R. (2005). Nuclear localization and chromatin targets of p21-activated kinase 1. J. Biol. Chem. *280*, 18130–18137.

Upla, P., Marjomäki, V., Kankaanpää, P., Ivaska, J., Hyypiä, T., Van Der Goot, F. G., and Heino, J. (2004). Clustering induces a lateral redistribution of $\alpha 2\beta 1$ integrin from membrane rafts to caveolae and subsequent protein kinase C-dependent internalization. Mol. Biol. Cell *15*, 625–636.

Upla, P., Marjomäki, V., Nissinen, L., Nylund, C., Waris, M., Hyypiä, T., and Heino, J. (2008). Calpain 1 and 2 are required for RNA replication of echovirus 1. J. Virol. *82*, 1581–1590.

Veithen, A., Amyere, M., Van Der Smissen, P., Cupers, P., and Courtoy, P. J. (1998). Regulation of macropinocytosis in v-Src-transformed fibroblasts: cyclic AMP selectively promotes regurgitation of macropinosomes. J. Cell Sci. *111*, 2329–2335.

Wadia, J. S., Stan, R. V., and Dowdy, S. F. (2004). Transducible TAT-HA fusogenic peptide enhances escape of TAT-fusion proteins after lipid raft macropinocytosis. Nat. Med. *10*, 310–315.

White, I. J., Bailey, L. M., Aghakhani, M. R., Moss, S. E., and Futter, C. E. (2006). EGF stimulates annexin 1-dependent inward vesiculation in a multivesicular endosome subpopulation. EMBO J. *25*, 1–12.

Xing, L., Huhtala, M., Pietiäinen, V., Kapyla, J., Vuorinen, K., Marjomäki, V., Heino, J., Johnson, M. S., Hyypiä, T., and Cheng, R. H. (2004). Structural and functional analysis of integrin alpha2I domain interaction with echovirus 1. J. Biol. Chem. *279*, 11632–11638.